



**HAL**  
open science

# Incipient short-circuit fault diagnosis of lithium-ion batteries

Jianwen Meng, Moussa Boukhniher, Claude Delpha, Demba Diallo

► **To cite this version:**

Jianwen Meng, Moussa Boukhniher, Claude Delpha, Demba Diallo. Incipient short-circuit fault diagnosis of lithium-ion batteries. *Journal of Energy Storage*, 2020, 31, pp.101658. 10.1016/j.est.2020.101658 . hal-02908249

**HAL Id: hal-02908249**

**<https://centralesupelec.hal.science/hal-02908249>**

Submitted on 22 Aug 2022

**HAL** is a multi-disciplinary open access archive for the deposit and dissemination of scientific research documents, whether they are published or not. The documents may come from teaching and research institutions in France or abroad, or from public or private research centers.

L'archive ouverte pluridisciplinaire **HAL**, est destinée au dépôt et à la diffusion de documents scientifiques de niveau recherche, publiés ou non, émanant des établissements d'enseignement et de recherche français ou étrangers, des laboratoires publics ou privés.



Distributed under a Creative Commons Attribution - NonCommercial 4.0 International License

# Incipient Short-Circuit Fault Diagnosis of Lithium-Ion Batteries

Jianwen MENG<sup>a,b</sup>, Moussa BOUKHNIFER<sup>c</sup>, Claude DELPHA<sup>d</sup>, Demba DIALLO<sup>a,e,\*</sup>

<sup>a</sup>*Université Paris-Saclay, CentraleSupélec, CNRS, GeePs, Sorbonne Université, 3-11 rue Joliot Curie, 91192 Gif-sur-Yvette, France*

<sup>b</sup>*ESTACA, Ecole d'Ingénieurs, 12 avenue Paul Delouvrier, 78066 Saint-Quentin-en-Yvelines, France*

<sup>c</sup>*Université de Lorraine, LCOMS, F-57000 Metz, France*

<sup>d</sup>*Université Paris-Saclay, CNRS, CentraleSupélec, Laboratoire des Signaux et Systèmes, 3 Rue Joliot Curie, 91192 Gif-sur-Yvette, France*

<sup>e</sup>*Shanghai Maritime University, 201306 Shanghai, China*

---

## Abstract

Diagnosing incipient short circuit (SC) of on-board lithium-ion cells is of great importance for safety operation, because it can prevent further deterioration such as spontaneous thermal runaway. Considering equivalent circuit models (ECMs) are currently the most used models for executing on-line battery state and parameter estimation, hence the purpose of this study is to propose a general battery incipient SC detection method through the commonly used ECMs. Model generality, design generality and implementation generality are the main design criteria. In this paper, inspired by the concept of Takagi-Sugeno fuzzy system, a weighting function self-regulating non-linear robust state and fault estimator that is designed for battery SC detection is proposed. Namely, the slowly changing characteristic of battery

---

\*Corresponding author

*Email address:* demba.diallo@geeeps.centralesupelec.fr (Demba DIALLO)

*Preprint submitted to Journal of Energy Storage*

*May 27, 2020*

state of charge (SOC) is fully taken into account to construct a weighting function self-regulating mechanism among different design segments. Genetic algorithm has been used for the membership function tuning. Therefore, incipient SC detection is addressed from the perspective of fault estimation. The absolute estimation error of battery SOC after the SC fault occurrence is smaller than 0.01 regardless of the SC resistance values. Furthermore, considering the estimated fault signal is usually corrupted with noise in reality, a statistical technique, namely Cumulative Sum, is employed to detect the tiny change of the signal due to the incipient fault. Theoretical and methodological contributions are the main aims of this research work. Intensive numerical simulations with real experimental data have verified the effectiveness of the proposed incipient SC detection method.

*Keywords:* Lithium-ion batteries, soft short circuit, incipient fault diagnosis, genetic algorithm (GA), cumulated sum (CUSUM)

---

## 1. Introduction

Fossil energy crisis and environmental issues are challenges for automobile industry and urge necessity developing alternatives to fuel-driven vehicles. Therefore, battery-driven electric and hybrid vehicles are becoming more and more attractive [1]. Thanks to their high energy/power density and extended life cycle, lithium-ion batteries (LIBs) are currently the state-of-the-art power sources for electrified powertrain systems [2].

Safety operation of LIBs is of vital importance for the development of electric vehicles (EVs). However, as resumed in [3], reliability and safety of electrified vehicle can be compromised due to overcharge (OC), overdischarge

(OD), internal short circuit (ISC) or external short circuit (ESC) of the battery. They can cause irreversible battery damages, or even lead to battery thermal runaway (TR), which is a catastrophic failure of on-board batteries.

Therefore, fault diagnosis and mitigation strategies for EVs' battery are critical functions to prevent TR. To this end, EVs' battery, typically consisting of hundreds to thousands of cells, is monitored by a battery management system (BMS). Data measurement, State-of-Charge (SOC), State-of-Health (SOH) and State-of-Power (SOP) estimation and fault diagnosis are the main functions of BMS [4, 5]. Its main function is to avoid battery OC and OD, but also prevent occurrence of thermal hazard [5, 6, 7, 8]. Because BMS requires on-line calculation with limited embedded computation resources, analytical models are usually preferred to data-driven approaches [9]. Battery fault detection and diagnosis has become a hotspot research topic in terms of BMS recently [10]. Battery short-circuit (external or internal) is a major concern as it is usually a precursor to thermal runaway. Hard short-circuit ( $m\Omega$  magnitude) will almost instantly lead to fire or explosion [11]. But in case of soft short-circuit ( $100/10/1 \Omega$ ) the thermal drift is going to be progressive. During this incubation period of the thermal runaway, no electrical or thermal thresholds are exceeded [12, 13] for a long time before any thermal accidents [11, 14]. So detection of soft short-circuit fault (denoted as incipient fault) at its earliest stage is meaningful as it can prevent battery failure. However soft short-circuit fault signature is weak as it may look like healthy operating conditions and fault features may be concealed in environmental nuisances. Therefore its detection is challenging.

Soft short-circuit (SC) detection can be, for instance, carried out by ther-

mal analysis. In [15], a 3D electrochemical-thermal model is built to simulate various ISC scenarios and ISC detection is addressed from model parameterization and parameter estimation perspective. In [16], residual-based battery thermal fault detection is achieved based on non-linear observers and a two-state thermal model. In [4], with voltage and temperature, ISC resistance is estimated based on electrical and thermal models. However, from security point of view, temperature-aware level often means that TR has already started [12]. Hence, battery SC diagnosis based on electrical signals, namely measured battery current and voltage, is more popular. In [12], soft SC diagnosis is done with the help of remaining charging capacity variation inside battery pack. In [11], ISC detection method for battery pack is proposed by identifying difference between cell model's parameters. In [17], a pseudo-two-dimensional model of micro ISC cells is proposed. The electrochemical model allows micro ISC mechanism analysis and impedance identification method of micro ISC cells is proposed. In [18, 19], physics-based model ESC detection scheme is proposed using different models for faulty and healthy conditions, which are obtained from experiments. In [20], according to time dependence of the capacity evaluation, ISC detection is evaluated while the cell is being charged. Furthermore, soft SC quantitative analysis is developed with cell difference model and state estimation algorithm in [21]. In [22], battery's multiple faults, including SC abuses, are isolated through battery chargers.

Although the aforementioned research works have recently contributed to soft SC diagnosis and detection, the methods are limited to one technology or are strongly dependent from one experimental test bed. The development of generic fault detection methods based on analytical models is relevant.

Generality of battery incipient SC detection method mainly refers to the following three points:

- *Model generality*: The development of a model that considers multi-physical phenomena, diversity of scales (microscopic to macroscopic), and diversity of materials (LMO( $\text{LiMn}_2\text{O}_4$ ), NMC ( $\text{LiNi}_x\text{Mn}_y\text{Co}_{1-x-y}\text{O}_2$ ) and LFP ( $\text{LiFePO}_4$ )) and configurations is a real challenge. An analytical model is usually adopted to develop control methods or/and monitoring techniques. This model should be flexible, parametrizable, and interoperable to cope with the diversity of batteries and the measurements (voltage, current, temperature) usually done at the battery (and not cell) level. Various experimental studies [13, 23, 24] have validated the Equivalent Circuit Model (ECM), commonly used for control and monitoring purposes. This model, when limited to 2 RC networks includes five parameters that can be identified with limited number of experiments. Besides, this model is interoperable because it can be combined with thermal and aging models that allow variations in these parameters to be taken into account. Therefore we have selected this 2 RC-network ECM to develop our incipient short-circuit detection method.
- *Design generality*: Design of incipient SC diagnosis method should not be constrained by experimental conditions. For example, with the effective battery fault diagnosis method proposed in [13], early warning of TR can be obtained. However, the faulty model must be tuned for each fault type and severity level requiring repeated experiments. Hence, we propose a soft SC diagnosis, taking advantage of the existing

literature, which includes validated model and experimental information. This method is designed to be adapted to different technologies and copes with different fault types and severity levels.

- *Implementation generality*: During battery operation, BMS can only collect current, voltage and temperature at given sampling frequency and accuracy[25]. Hence, battery incipient SC fault features should be retrieved from this information. Besides, an easy-to-understand fault diagnosis structure is more attractive.

Therefore, the development of battery SC incipient diagnosis method presented in this paper relies on the three aforementioned criteria. The novelty and original contributions of this paper are:

- Based on battery ECM, battery incipient SC fault diagnosis is addressed from the perspective of fault estimation. Inspired by the concept of Takagi-Sugeno fuzzy system, we propose a weighting function self-regulating state and fault estimator that is designed for battery SC detection.
- Taking into account the slowly changing characteristic of battery SOC and using a genetic algorithm, we propose a systematic approach to construct the self-regulating mechanism to cope with the non-linear battery OCV (open circuit voltage)-SOC curve.
- To detect tiny changes in the fault feature, which are usually hidden in the environmental noise, we have combined statistical information (Cumulative Sum) with the model-based observer fault estimation.

The rest of the paper is structured as follows. Firstly, to model the short-circuit (ISC or ESC), a resistance is connected in parallel to a healthy battery ECM. This faulty model is introduced in section II. Then, to achieve soft SC diagnosis from the perspective of control, a systematic way of designing the weighting function self-regulating battery fault estimator is proposed in section III. In addition, numerical simulations with real experimental data are presented in section IV. Furthermore, CUmulative SUM (CUSUM) is used to retrieve the fault information from the estimated fault. Finally, a conclusion ends the paper.

## 2. Battery ECM with SC resistance

As shown in Fig. 1, both internal SC (ISC) and external SC (ESC) are modelled as a healthy battery ECM connected in parallel with a resistance  $R_{sc}$  [26].

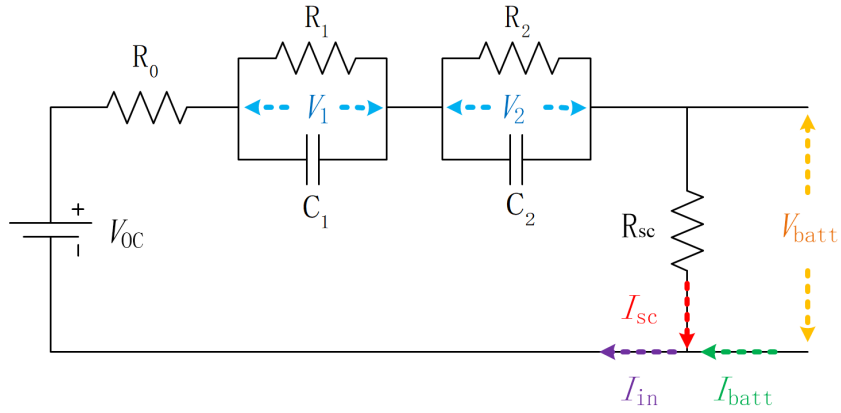


Figure 1: Battery ECM with SC resistance.

### 2.1. ECM description

1. The resistor  $R_0$  stands for the ohmic resistance which includes resistance of contacts, electrodes as well as electrolytes [24].
2. The double pair RC characterizes charge transfer effect, diffusion effect and double-layer behavior inside LIBs. It simulates battery's transient response. Besides, the double RC-network is a good trade-off between model error and model complexity compared with single-RC and triple-RC structures [27].
3. The voltage source  $V_{OC}$  represents OCV, which mainly depends on battery SOC [28]. As shown in Fig. 2, its average value,  $V_{OC}(soc)$ , is usually a non-linear monotonically [29] increasing function of SOC. In each SOC interval, it can be approximated by  $V_{OC_i}(soc) = a_i \cdot soc + b_i$  ( $a_i$  and  $b_i$  are constant in the  $i$ -th SOC interval).

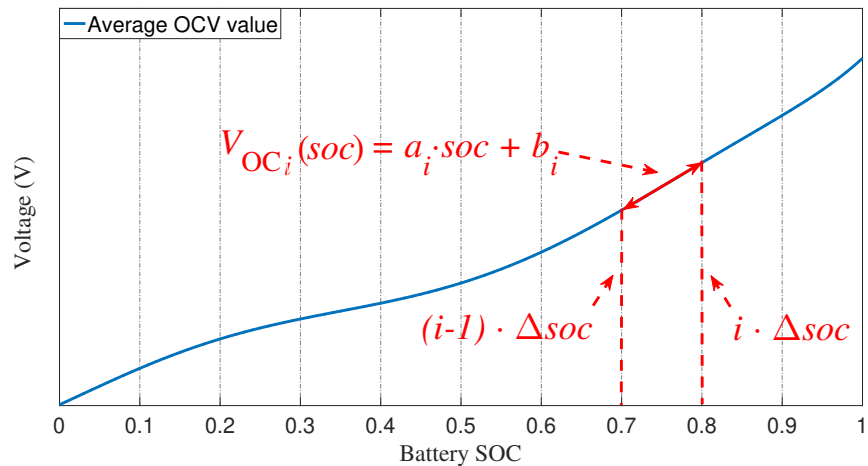


Figure 2: General shape of average OCV curve (example adapted from [24]).

4.  $V_1$  and  $V_2$  are voltages across capacitors  $C_1$  and  $C_2$  respectively.  $V_{\text{batt}}$  is battery terminal voltage.
5.  $I_{\text{batt}}$  is battery load current. According to its reference direction in Fig. 1, “+” means discharging process, while “-” means charging process.
6.  $I_{\text{sc}}$  is SC current flowing into equivalent SC resistance  $R_{\text{sc}}$ . It is unidirectional and obviously unknown. Furthermore, its value is  $I_{\text{sc}} = \frac{V_{\text{batt}}}{R_{\text{sc}}}$ .
7. According to Kirchhoff’s circuit law,  $I_{\text{in}} = I_{\text{batt}} + I_{\text{sc}}$ , is battery real input current with or without SC fault. If  $R_{\text{sc}}$  approaches to infinity, then  $I_{\text{sc}} \approx 0$  and  $I_{\text{in}} \approx I_{\text{batt}}$ . Therefore, battery operates in healthy condition. Otherwise, battery is exposed to SC conditions, which could be induced by ISC or ESC.

## 2.2. Battery modelling

Firstly, battery SOC  $\in [0\%, 100\%]$  can be modelled by the classical Coulomb counting method [24]:

$$\text{soc}(t) = \text{soc}(t_0) - \eta \int_{t_0}^t \frac{I_{\text{batt}}(\tau)}{C_n} d\tau \quad (1)$$

where,  $\text{soc}$  is the operator of SOC;  $\eta$  is Columbic efficiency usually approximated to 1 for LIBs;  $C_n$  (Ah: Ampere-hour) is battery nominal capacity;  $\text{soc}(t)$  is required SOC at time point  $t$  based on its initial value  $\text{soc}(t_0)$ .

Therefore, using Kirchhoff’s law, battery dynamic model can be described by the following discrete state-space representation:

$$\begin{bmatrix} V_1(k+1) \\ V_2(k+1) \\ soc(k+1) \end{bmatrix} = \mathbf{A} \begin{bmatrix} V_1(k) \\ V_2(k) \\ soc(k) \end{bmatrix} + \mathbf{B}I_{in}(k) \quad (2)$$

$$V_{batt}(k) = V_{OC}(soc) - V_1(k) - V_2(k) - R_0I_{in}(k)$$

where,

$$\mathbf{A} = \begin{bmatrix} e^{\frac{-T}{R_1C_1}} & 0 & 0 \\ 0 & e^{\frac{-T}{R_2C_2}} & 0 \\ 0 & 0 & 1 \end{bmatrix}, \quad \mathbf{B} = \begin{bmatrix} R_1 \cdot (1 - e^{\frac{-T}{R_1C_1}}) \\ R_2 \cdot (1 - e^{\frac{-T}{R_2C_2}}) \\ \frac{-\eta T}{C_n} \end{bmatrix}$$

Eq. (2) is obtained with the zero-order hold approximation under the assumption that  $I_{in}$  is constant between two adjacent sampling points. The sampling period,  $T = 1$  s in this study.

### 3. Weighting function self-regulating fault estimator

The OCV-SOC curve is non-linear. However the battery can be described as a linear time-invariant (LTI) model in each SOC interval. This assumption is supported with experimental verification conducted in [13, 24, 27, 30]. Therefore, inspired by the concept of Takagi-Sugeno (TS) fuzzy system, a systematic way to blend the linear intervals of OCV-SOC curve and build the weighting function self-regulating fault estimator is proposed. The principle of TS fuzzy system, including modeling and observer/controller design process, is to study nonlinear systems by a set of local LTI models. These models are interpolated using non-linear weighting functions or membership

functions (MFs). This mechanism allows the fusion of all the linear subsystems [31]. The general design process is shown in Fig. 3, and details will be given in the following.

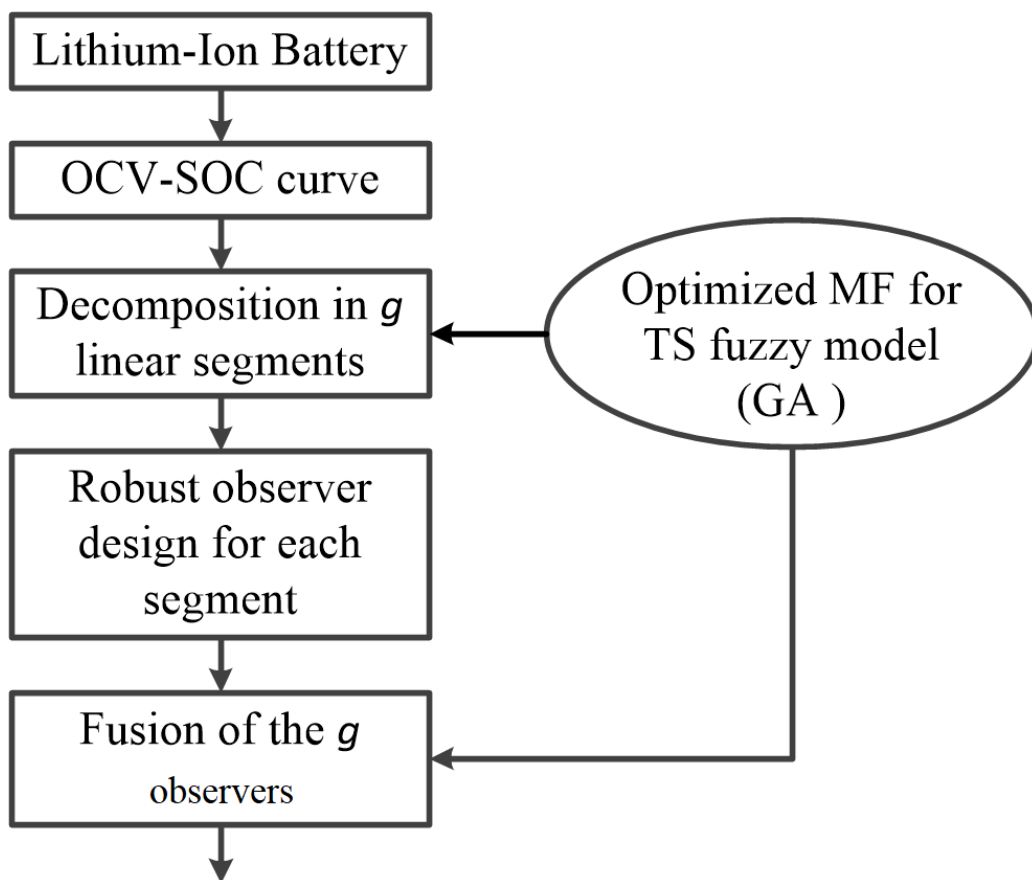


Figure 3: Flowchart for robust observer design.

### 3.1. Fuzzification of OCV-SOC curve

The flowchart presented in Fig. 4 illustrates the fuzzification process for battery OCV-SOC curve:

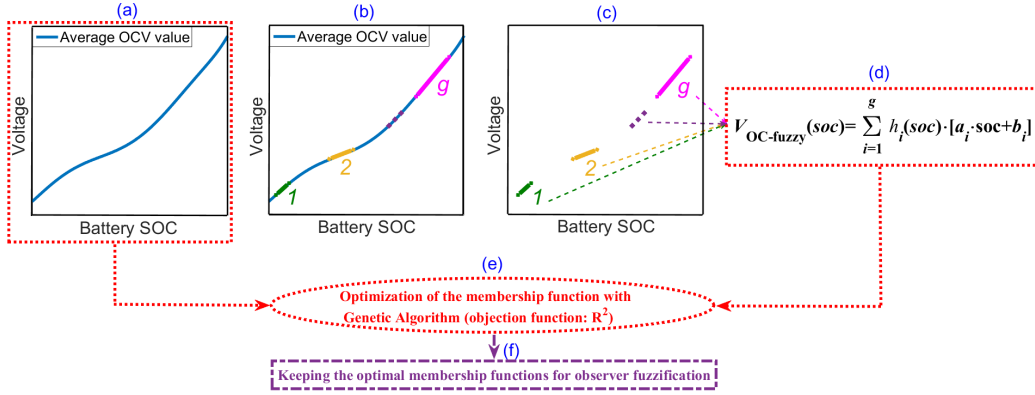


Figure 4: Flowchart of fuzzification process for battery OCV-SOC curve

- Fig. 4(b): we consider  $g$  ( $g \in \mathbb{N}$  and  $g \geq 2$ ) linear segments from the OCV-SOC curve and fit the corresponding mathematical expression for each linear segment as (3). Note that determination of  $g$  depends on the nonlinearity level of OCV-SOC curve.

$$V_{OC_i}(soc) = a_i \cdot soc + b_i, \quad (i = 1, \dots, g) \quad (3)$$

It is important to notice that the linear segments do not need to be contiguous. This approach has two main advantages. Firstly, the model is much simpler compared to the classical one which uses a small discretization step [29]. Secondly, the model is robust because it does not require a strong approximation of the linearity of the whole curve.

- Fig. 4(c): a MF should be distributed to each linear segment based on the main idea of TS fuzzy system. In other words, each linear segment contributes to the global nonlinear behavior of OCV-SOC curve through a weighting function  $\pi(soc)$ . Furthermore, in order to have a smooth transition among different linear segments,  $\pi$  is selected as

Gaussian type. As a result,  $\pi(soc)$  is determined by its mean  $\mu$  and its variance  $\sigma^2$ . Hence, for any value of SOC, it is supposed that

$$\pi_i(soc) \geq 0 \text{ and } \sum_{i=1}^g \pi_i(soc) > 0, \quad (i = 1, \dots, g)$$

- Fig. 4(d): after these two steps, OCV-SOC curve can be expressed as (4).

$$V_{\text{OC-fuzzy}}(soc) = \sum_{i=1}^g h_i(soc) \cdot [a_i \cdot soc + b_i] \quad (4)$$

where,  $h_i(soc) = \frac{\pi_i(soc)}{\sum_{i=1}^g \pi_i(soc)}$ . Hence, for any value of SOC,  $h_i(soc)$  satisfies

$$h_i(soc) \geq 0 \text{ and } \sum_{i=1}^g h_i(soc) = 1, \quad (i = 1, \dots, g)$$

- Fig. 4(e): selecting the optimal pair  $(\mu_i, \sigma_i^2)$  ( $i = 1, \dots, g$ ) for each MF  $\pi_i$  ( $i = 1, \dots, g$ ) is necessary. This optimization problem is similar to curve fitting. Therefore, coefficient of determination,  $R^2$ , used as the optimization criterion is formulated in (5).

$$R^2 = 1 - \frac{\sum_{i=1}^{n_{ocv}} [V_{\text{OC}}(soc) - V_{\text{OC-fuzzy}}(soc)]^2}{\sum_{i=1}^{n_{ocv}} [V_{\text{OC}}(soc) - \bar{V}_{\text{OC}}(soc)]^2} \quad (5)$$

where,  $\bar{V}_{\text{OC}}(soc) = \frac{1}{n_{ocv}} \sum_{i=1}^{n_{ocv}} [V_{\text{OC}}(soc)]$ ;  $n_{ocv}$  is the number of data points used in the optimization process;  $V_{\text{OC}}(soc)$  is the original average OCV-SOC data as shown in Fig. 4(a). Finally, as indicated in Fig. 4(f), the obtained optimal membership functions after the optimization process will be used later for observer fusion.

### 3.2. Fuzzification of robust observers

Due to the relationship  $I_{\text{in}} = I_{\text{batt}} + I_{\text{sc}}$ , the mathematical representation of the battery ECM with SC resistance in the  $i$ -th SOC interval can be arranged as:

$$\mathbf{x}(k+1) = \mathbf{A}\mathbf{x}(k) + \mathbf{B}I_{\text{batt}}(k) + \mathbf{B}_f I_{\text{sc}}(k) \quad (6)$$

$$y(k) = \mathbf{C}\mathbf{x}(k) + DI_{\text{batt}}(k) + D_f I_{\text{sc}}(k)$$

where,  $\mathbf{B}_f = \mathbf{B}$ ;  $\mathbf{C} = [-1 \quad -1 \quad a_i]$ ;  $D = D_f = -R_0$ . State vector is  $\mathbf{x}(k) = [V_1(k), V_2(k), \text{soc}(k)]'$ ; model output is  $y(k) = V_{\text{batt}}(k) - b_i$ .

According to (6), the design process of battery fault estimator is discussed based on [32]. Firstly, considering modeling error and measurement noise, battery SC model (6) can be further generalized to (7), where both state equations and output equation will be studied with bounded disturbance.

$$\mathbf{x}(k+1) = \mathbf{A}\mathbf{x}(k) + \mathbf{B}u(k) + \mathbf{B}_f f(k) + \mathbf{B}_d d(k) \quad (7)$$

$$y(k) = \mathbf{C}\mathbf{x}(k) + Du(k) + D_f f(k) + D_d d(k)$$

where,  $\mathbf{x}(k) \in \mathbb{R}^n$  is the state vector;  $y(k) \in \mathbb{R}^p$  is the output;  $u(k) \in \mathbb{R}^m$  is the known input, which corresponds to  $I_{\text{batt}}$ ;  $f(k) \in \mathbb{R}^{n_f}$  is the so-called fault, which corresponds to  $I_{\text{sc}}$ ;  $d(k) \in \mathbb{R}^{n_d}$  is the disturbance that belongs to  $l_2[0, \infty]$ ;  $\mathbf{B}_d$  and  $D_d$  are constant real matrices of appropriate dimensions.

Furthermore, fault estimator (8) is designed as a proportional-integral observer. Not only the integral term can guarantee a robust state estimation at fault occurrence, but it can also provide fault estimation simultaneously [33].

$$\begin{aligned} \hat{\mathbf{x}}(k+1) &= \mathbf{A}\hat{\mathbf{x}}(k) + \mathbf{B}u(k) + \mathbf{B}_f \hat{f}(k) - \mathbf{L} \cdot (\hat{y}(k) - y(k)) \\ \hat{f}(k+1) &= \hat{f}(k) - F \cdot (\hat{y}(k) - y(k)) \\ \hat{y}(k) &= \mathbf{C}\hat{\mathbf{x}}(k) + Du(k) + D_f \hat{f}(k) \end{aligned} \quad (8)$$

where  $\hat{\boldsymbol{x}}(k) \in \mathbb{R}^n$  is the estimated state vector;  $\hat{y}(k) \in \mathbb{R}^p$  is the observer output;  $\hat{f}(k) \in \mathbb{R}^{n_f}$  is the estimated  $f(k)$ ;  $\boldsymbol{L} \in \mathbb{R}^{n \times p}$  and  $F \in \mathbb{R}^{n_f \times p}$  are observer gains.

Therefore, the error dynamics between model (7) and observer (8) can be described as (9),

$$\bar{\boldsymbol{e}}(k+1) = (\bar{\boldsymbol{A}}_D - \bar{\boldsymbol{L}}\bar{\boldsymbol{C}})\bar{\boldsymbol{e}}(k) + (\bar{\boldsymbol{L}}\bar{\boldsymbol{D}}_d - \bar{\boldsymbol{B}}_d)\bar{\boldsymbol{v}}_D(k) \quad (9)$$

where

$$\bar{\boldsymbol{A}}_D = \begin{bmatrix} \boldsymbol{A} & \boldsymbol{B}_f \\ 0_{n_f \times n} & I_{n_f} \end{bmatrix}, \bar{\boldsymbol{B}}_d = \begin{bmatrix} \boldsymbol{B}_d & 0_{n \times n_f} \\ 0_{n_f \times n_d} & I_{n_f} \end{bmatrix}$$

$$\bar{\boldsymbol{C}} = \begin{bmatrix} \boldsymbol{C} & D_f \end{bmatrix}, \bar{\boldsymbol{D}}_d = \begin{bmatrix} D_d & 0_{p \times n_f} \end{bmatrix}$$

$$\bar{\boldsymbol{e}}(k) = \begin{bmatrix} \boldsymbol{e}_x(k) \\ e_f(k) \end{bmatrix}, \bar{\boldsymbol{v}}_D(k) = \begin{bmatrix} d(k) \\ \Delta f(k) \end{bmatrix}$$

and  $\bar{\boldsymbol{L}} = \begin{bmatrix} \boldsymbol{L} & F \end{bmatrix}'$ .  $\boldsymbol{e}_x(k) = \hat{\boldsymbol{x}}(k) - \boldsymbol{x}(k)$ ,  $e_f(k) = \hat{f}(k) - f(k)$ ;  $\Delta f(k) = f(k+1) - f(k)$  belongs to  $l_2[0, \infty)$ .  $I_i$  is the symbol of unit matrix with  $i \times i$  dimension. 0 is zero matrix with corresponding dimension.

The design of the observer is how to determine  $\bar{\boldsymbol{L}}$  to make the error dynamics (9) satisfy the following two objectives [32]:

- $(\bar{\boldsymbol{A}}_D - \bar{\boldsymbol{L}}\bar{\boldsymbol{C}})$  is Hurwitz stable. Its eigenvalues are inside the unit circle for discrete-time system.
- the fault estimation error  $e_f(k)$  is insensitive to  $\bar{\boldsymbol{v}}_D(k)$ , namely,  $e_f(k)$  is as small as possible.

In order to achieve the aforementioned objectives, a multi-constrained design method is proposed in [32]. The main results are shown directly in **Theorem**, which will be used to design the fault estimator.

**Theorem.** *Let a prescribed  $H_\infty$  performance level  $\gamma$  and a circular region  $\mathcal{D}(\alpha, r)$  be given. If there exist two symmetric positive definite matrices  $\bar{\mathbf{P}}_1, \bar{\mathbf{P}}_2 \in \mathbb{R}^{(n+n_f) \times (n+n_f)}$  and two matrices  $\bar{\mathbf{S}} \in \mathbb{R}^{(n+n_f) \times (n+n_f)}$ ,  $\bar{\mathbf{Y}} \in \mathbb{R}^{(n+n_f) \times p}$  such that the following conditions hold:*

$$\begin{bmatrix} \bar{\mathbf{M}} & \bar{\mathbf{N}} & \bar{\mathbf{Y}}\bar{\mathbf{D}}_d - \bar{\mathbf{S}}\bar{\mathbf{B}}_d & 0 \\ * & -\bar{\mathbf{P}}_1 & 0 & \bar{\mathbf{I}}_{n_f} \\ * & * & -\gamma\mathbf{I}_{(n_d+n_f)} & 0 \\ * & * & * & -\gamma\mathbf{I}_{n_f} \end{bmatrix} < 0 \quad (10)$$

and

$$\begin{bmatrix} -\bar{\mathbf{S}} - \bar{\mathbf{S}}' + \bar{\mathbf{P}}_2 & \bar{\mathbf{S}}\bar{\mathbf{A}}_D - \bar{\mathbf{Y}}\bar{\mathbf{C}} - \alpha\bar{\mathbf{S}} \\ * & -r^2\bar{\mathbf{P}}_2 \end{bmatrix} < 0 \quad (11)$$

where  $\bar{\mathbf{I}}_{n_f} = \begin{bmatrix} 0_{n \times n_f} \\ \mathbf{I}_{n_f} \end{bmatrix}$ ,  $\bar{\mathbf{M}} = -\bar{\mathbf{S}} - \bar{\mathbf{S}}' + \bar{\mathbf{P}}_1$ ;  $\bar{\mathbf{N}} = \bar{\mathbf{S}}\bar{\mathbf{A}}_D - \bar{\mathbf{Y}}\bar{\mathbf{C}}$ ; “\*” represents the matrix’s symmetric term. Then error dynamics (9) satisfies the  $H_\infty$  performance index  $\|e_f(k)\|_2 < \gamma\|\bar{\mathbf{v}}_D\|_2$ , the eigenvalues of  $(\bar{\mathbf{A}}_D - \bar{\mathbf{L}}\bar{\mathbf{C}})$  belong to  $\mathcal{D}(\alpha, r)$ , and the gain matrix  $\bar{\mathbf{L}}$  is given by  $\bar{\mathbf{L}} = \bar{\mathbf{S}}^{-1}\bar{\mathbf{Y}}$ .

To be short, the linear fault estimator design is subject to two linear-matrix-inequalities (LMIs). The  $H_\infty$  performance and regional pole constraint constitute the so-called multi-constrained design method [32]. The observer performance is adjusted by tuning the circular region  $\mathcal{D}(\alpha, r)$ .

Hence, according to the previously presented method, at first a robust observer is built for each linear segment. Namely, the gain vector  $\bar{\mathbf{L}}_i = \begin{bmatrix} \mathbf{L}_i & F_i \end{bmatrix}'$  ( $i = 1, \dots, g$ ) for each sub-observer is determined. Then, based on (8),  $g$  linear robust observers can be blended directly as (12), where the subscript  $(\cdot)_{\text{fuzzy}}$  stands for elements of TS fuzzy observer.

$$\begin{aligned}
\hat{\mathbf{x}}_{\text{fuzzy}}(k+1) &= \sum_{i=1}^g h_i(\widehat{\text{soc}}_{\text{fuzzy}}(k)) [\mathbf{A} \hat{\mathbf{x}}_{\text{fuzzy}}(k) + \mathbf{B}u(k) + \mathbf{B}_f \hat{f}_{\text{fuzzy}}(k) \\
&\quad - \mathbf{L}_i \cdot (\hat{y}_{\text{fuzzy}}(k) - y(k))] \\
\hat{f}_{\text{fuzzy}}(k+1) &= \sum_{i=1}^g h_i(\widehat{\text{soc}}_{\text{fuzzy}}(k)) \left[ \hat{f}_{\text{fuzzy}}(k) - F_i \cdot (\hat{y}_{\text{fuzzy}}(k) - y(k)) \right] \\
\hat{y}_{\text{fuzzy}}(k) &= \sum_{i=1}^g h_i(\widehat{\text{soc}}_{\text{fuzzy}}(k)) \left[ \mathbf{C} \hat{\mathbf{x}}_{\text{fuzzy}}(k) + Du(k) + D_f \hat{f}_{\text{fuzzy}}(k) \right]
\end{aligned} \tag{12}$$

Two important points should be pointed out. Firstly, according to TS fuzzy system design method, the optimal MFs for the different linear observers are exactly the same ones as those in the fuzzification process of battery OCV-SOC curve [31]. Secondly,  $\frac{d\text{soc}}{dt} \approx 0$  has been proven both in theory and practice [34, 35]. Namely, the slowly changing characteristic of SOC makes  $\widehat{\text{soc}}_{\text{fuzzy}}(k+1) \approx \widehat{\text{soc}}_{\text{fuzzy}}(k)$ , where  $\widehat{\text{soc}}_{\text{fuzzy}}(k)$  is included in the estimated state vector  $\hat{\mathbf{x}}_{\text{fuzzy}}(k)$ . Therefore,  $\widehat{\text{soc}}_{\text{fuzzy}}(k)$  is the so-called fuzzy variable in the TS fuzzy observer for battery ECM, and the obtained TS fuzzy observer is, in essence, a weighting function self-regulating robust observer. The obtained TS fuzzy observer is schematic diagram is represented in Fig. 5.

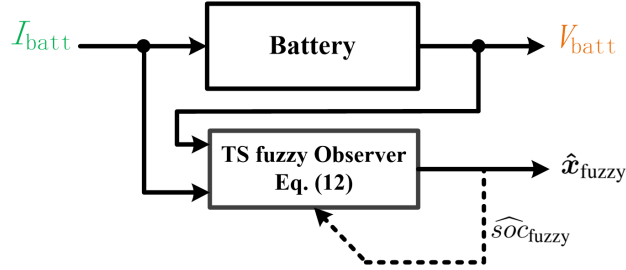


Figure 5: Weight function self-regulating fault estimator.

#### 4. Numerical simulations

Numerical simulations of TS fuzzy fault estimator will be given in this section based on SAMSUNG ICR 18650-22P LIB cell. Its basic electrical characteristics are summarized in Table 1 [30].

Table 1: Electrical characteristics of SAMSUNG ICR 18650-22P cell

Nominal capacity	2150 mAh
Nominal voltage	3.6 V
Charging cut-off voltage (100% SOC)	4.2±0.05 V
Discharging cut-off voltage (0% SOC)	2.75 V
Maximum charge current	2150 mA
Maximum discharge current	10 A

Battery ECM parameters are shown in Table 2. All the parameters are obtained at 20 °C. The details for parameter identification can be found in [30].

In addition, according to our research interest and the electrical charac-

Table 2: SAMSUNG ICR 18650-22P LIB cell parameters

$R_0$ ( $\Omega$ )	0.0395
$R_1$ ( $\Omega$ )	0.0107
$R_2$ ( $\Omega$ )	0.0031
$C_1$ (F)	4721.2
$C_2$ (F)	17288
$C_n$ (mAh)	2150
$V_{OC}(soc)$	$-0.6195soc^4 + 1.0899soc^3 - 0.3539soc^2 + 0.6196soc + 3.2354$

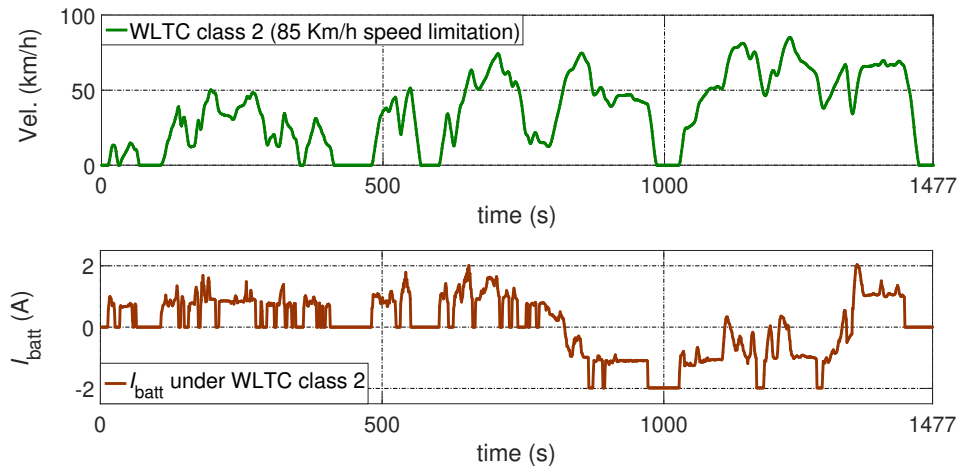


Figure 6: EV test cycle and the corresponding adapted EV battery cell current response.

teristics of SAMSUNG ICR 18650-22P LIB cell, the input current for battery ECM is adapted from real experimental Tazzari Zero EV of university of Lille 1 in France [36]. It is a fuel cell/battery hybrid EV with a maximum speed of 85 km/h. Ignoring its fuel cell/battery architecture and energy management strategy, we only focus on the battery current response.

Therefore, in order to simulate battery typical operating condition, WLTC2 (Worldwide harmonized Light-duty vehicles Test Cycle: class 2) is selected as test cycle. Speed profile and corresponding battery response adapted to SAMSUNG ICR 18650-22P LIB cell are shown in Fig. 6.

Statistical information on the disturbance refers to [27]. Process and measurement nuisances are assumed to be independent additive white Gaussian noises (AWGN). Their variances are  $1 \times 10^{-8}$  and  $3.6 \times 10^{-5}$  respectively. Therefore, in order to determine the disturbance mapping matrices  $\mathbf{B}_d$  and  $D_d$ , the disturbance term  $d$  is supposed to follow a standard normal distribution with a variance of 1. Hence,  $\mathbf{B}_d = [1 \times 10^{-4}, 1 \times 10^{-4}, 1 \times 10^{-4}]'$  and  $D_d = 0.006$  consequently.

#### 4.1. Short-circuit effect

Firstly, with 24 cycles of WLTC 2, healthy battery electrical response and battery electrical response under different soft SC conditions are shown in Fig. 7. Different soft SC resistances, 10  $\Omega$ , 50  $\Omega$  and 100  $\Omega$ , are respectively introduced into the battery ECM in the middle of the total test time.

As it can be observed from Fig. 7, battery electrical behavior under soft SC conditions is almost similar to a healthy battery because both voltage and SOC are in normal operation ranges according to Table 1. But the underlying effects of incipient faults compromise battery's safety and reliability.

Especially when battery is controlled in closed-loop EV power supply system, battery SOC will be maintained in its normal range by the energy management strategy that ignores the actual battery status [6]. Therefore, battery condition will keep on deteriorating before TR. Hence, soft SC detection is critical, especially when it is hard to distinguish from the healthy situation.

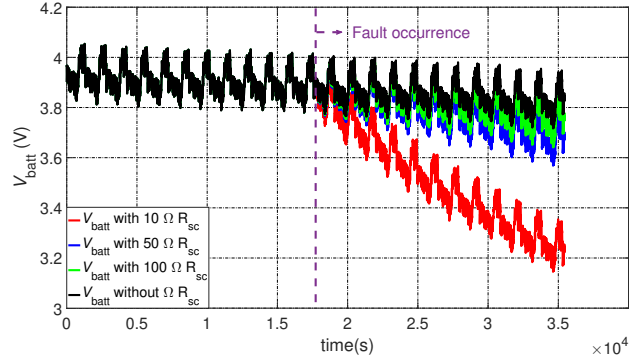
#### 4.2. Short-circuit current estimation

Following the design process presented in section III, the selected SOC ranges, the corresponding linear robust observer design results and the optimal MF parameters (mean and variance) are shown in Table 3. Furthermore, the shape of the optimized MFs and the fuzzification result of OCV-SOC curve are shown in Fig. 8.

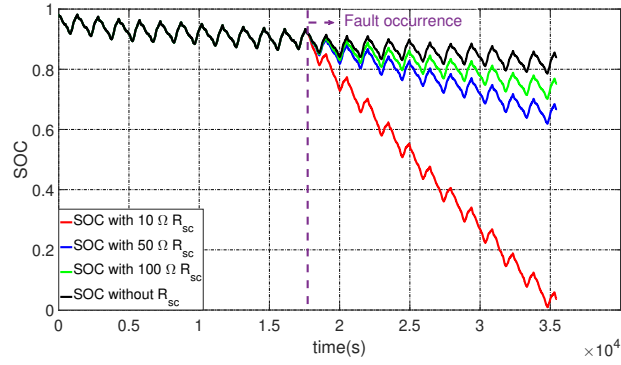
Figure 9 displays estimation results of the proposed observer under 10  $\Omega$ 's SC resistance with 24 cycles of WLTC2. The 10  $\Omega$  resistance modelling SC fault is introduced into the battery ECM at the 12th test cycle. The estimator converges although the initial value is smaller than the actual one. Especially after the abrupt fault occurrence, the estimator is able to track the dynamic change of the battery SOC. Furthermore, as it can be observed from Fig. 9(g), fault estimation is a valuable fault indicator.

Table 3: Linear robust SOC observer design and MF optimization results

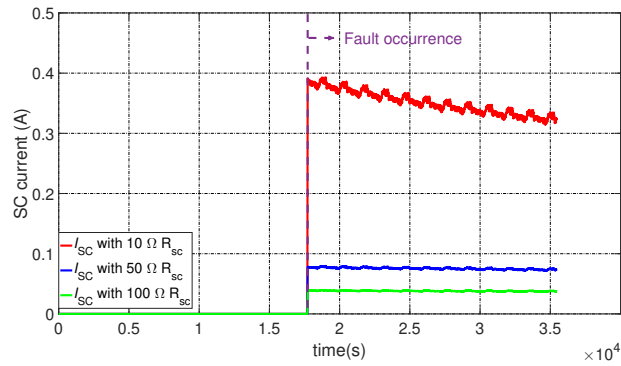
SOC Range \ Term	Linearization	$\bar{L}$	$\gamma$	$\mathcal{D}(\alpha, r)$	$(\mu, \sigma^2)$
[0, 0.2]	0.5841* <i>soc</i> +3.2362	[-0.0013, 0.0024, 0.0024, -10.1235]'	2.5046	(0.8, 0.2)	(0.19999, 0.09753)
[0.65, 0.85]	0.8779* <i>soc</i> +3.1064	[-0.0020, 0.0017, 0.0023, -10.1241]'	2.5046	(0.8, 0.2)	(0.8499, 0.05767)
[0.98, 1]	0.7190* <i>soc</i> +3.2525	[-0.0017, 0.0020, 0.0024, -10.1233]'	2.5046	(0.8, 0.2)	(0.99999, 0.11031)



(a)  $V_{\text{batt}}$



(b) Battery SOC



(c) Amplitude of  $I_{\text{sc}}$

Figure 7: Battery electrical response under different SC conditions

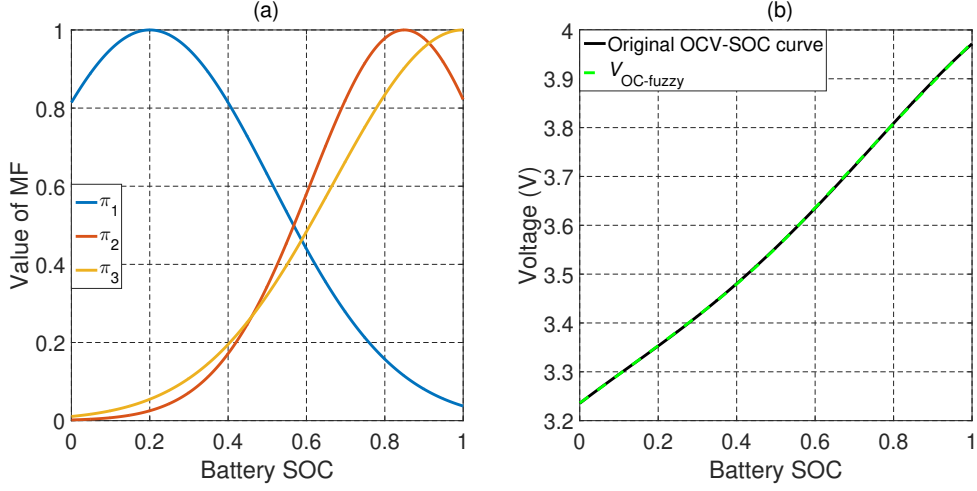
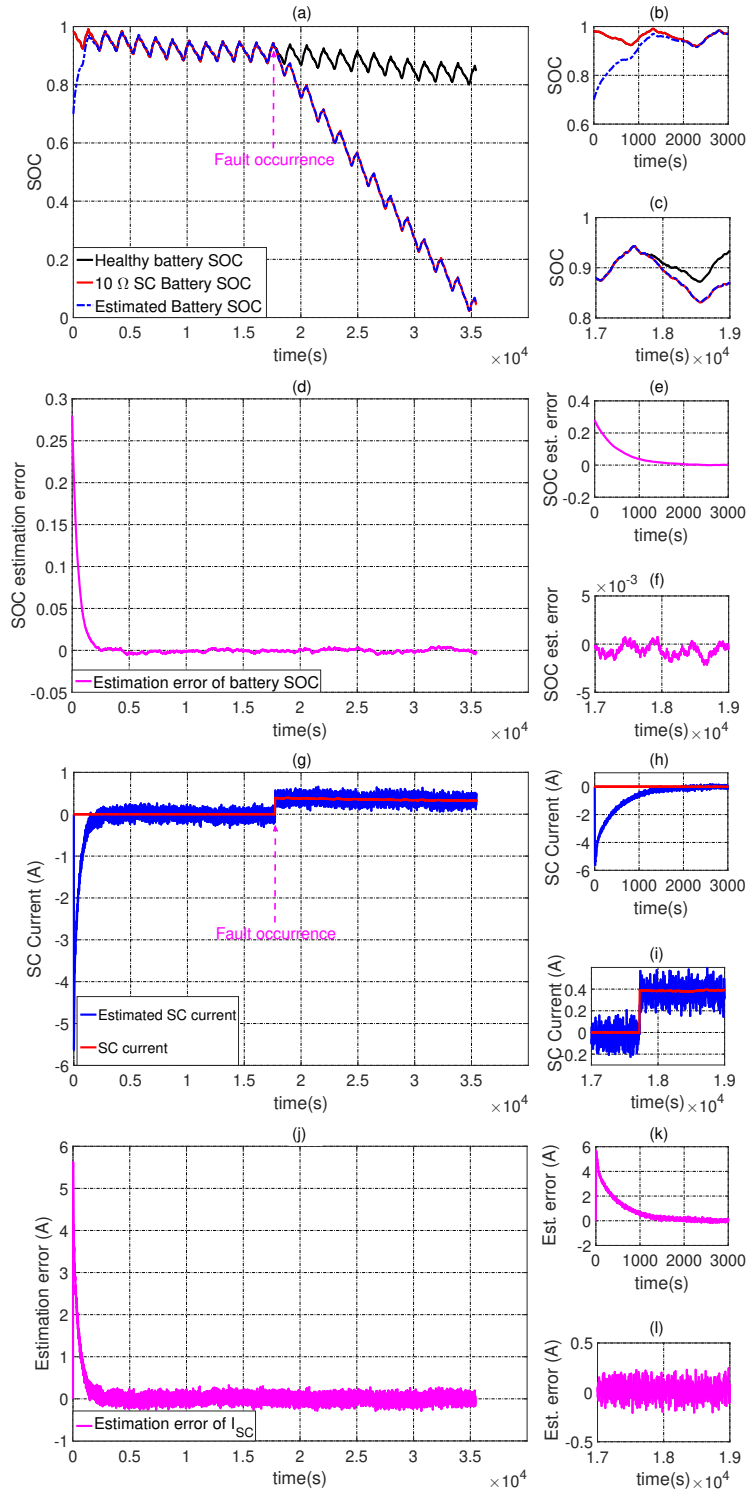


Figure 8: (a) Optimized MF for each linear segment; (b) Fuzzification result of the OCV-SOC curve.

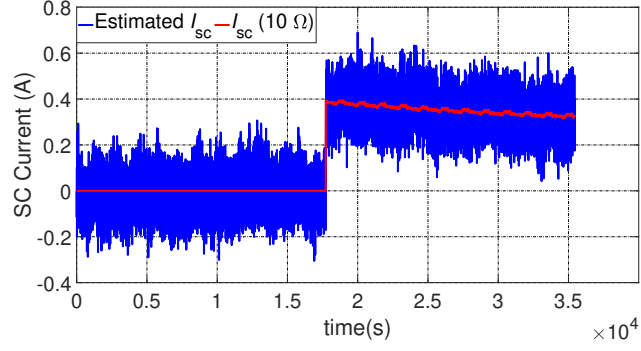
However, as shown in Fig. 10, when SC current amplitude is small, namely the SC fault is small, it is difficult to distinguish the healthy and faulty modes from the estimated  $I_{sc}$ . Because fault signal is corrupted with noise.

## 5. Statistical analysis

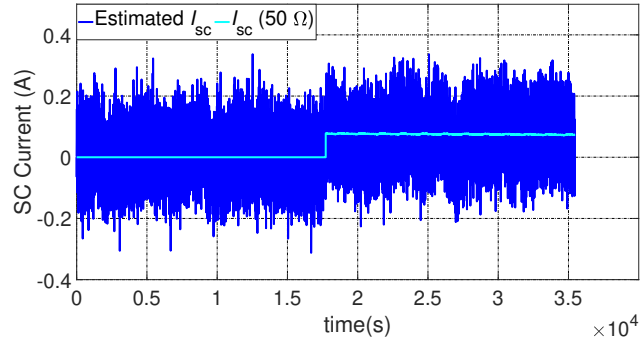
As it can be observed from the intensive numerical simulations, fault information is concealed in the noise and it is worse when the fault is more and more incipient ( $R_{sc} > 100\Omega$ ). To assess fault occurrence based on probabilities, we will use statistical analysis of the estimated signal. The randomness in the data is introduced through Monte-Carlo method with a high number of repetitive simulations with randomized noise samples but with the same distribution parameters. In the following, the  $I_{sc}$  estimation is done 500 times for each condition (healthy or faulty). The first four statistical



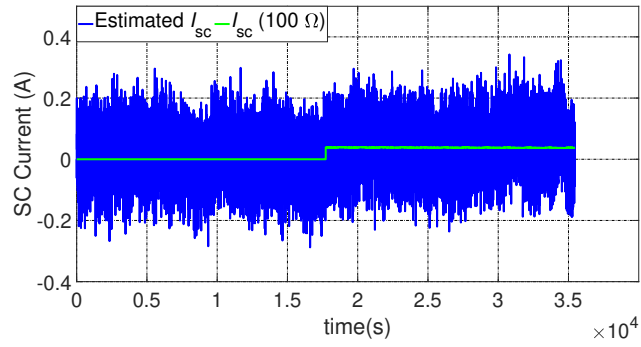
24  
 Figure 9: (a) SOC estimation result; (b) enlargement of the beginning; (c) dynamic estimation performance after fault occurrence; (d)/(e)/(f) estimation error corresponding to (a)/(b)/(c); (g) SC current estimation result; (h) enlargement of the beginning; (i) dynamic estimation performance after fault occurrence; (j)/(k)/(l) estimation error corresponding to (g)/(h)/(i).



(a)  $I_{sc}$  estimation result ( $R_{sc} = 10\Omega$ )



(b)  $I_{sc}$  estimation result ( $R_{sc} = 50\Omega$ )



(c)  $I_{sc}$  estimation result ( $R_{sc} = 100\Omega$ )

Figure 10:  $I_{sc}$  estimation result under different SC conditions

moments namely mean, variance, skewness and kurtosis of  $\hat{I}_{sc}$ , are calculated both for healthy and faulty cases. As it can be observed from Fig. 11, only the mean value exhibits significant change after fault occurrence.

### 5.1. CUSUM fault detection

Based on the statistical analysis result in the previous section, Cumulative Sum (CUSUM) will be applied on the mean value on the estimated  $I_{sc}$  to improve incipient SC fault detection performances.

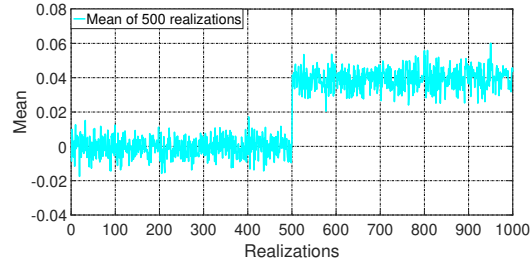
Flowchart of battery soft SC detection method proposed in this paper is displayed in Fig. 12.

CUSUM is a well-known statistical technique [37] that has already been proved to be efficient in detecting abrupt changes [38]. The CUSUM function, denoted  $S$  in the following, is a simple detection algorithm based on the likelihood process [38]. Namely, the estimated SC current will be treated as time-series signal, and then, the CUSUM method is used to detect small changes in the signal due to the incipient fault. Theoretically, based on Gaussian distributed process, it is optimally derived as the sufficient statistics  $s_k$  such as [38]:

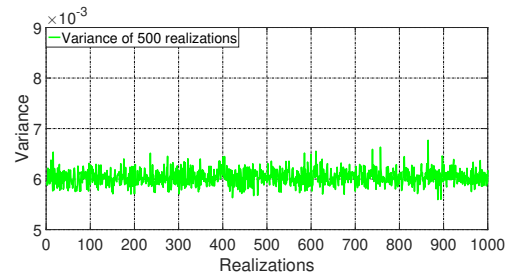
$$S_N = \sum_{k=1}^N s_k \quad (13)$$

where  $N$  is the number of samples. And according to the statistical analysis for the estimated  $I_{sc}$ ,  $s_k$  is considered in the case of mean changes in (14) [38]:

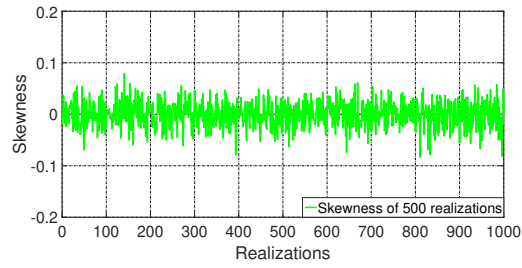
$$s_k = \left( \frac{\mu_f - \mu_h}{\sigma_h^2} \right) \times \left( \hat{I}_{sc}(k) - \frac{\mu_f + \mu_h}{2} \right) \quad (14)$$



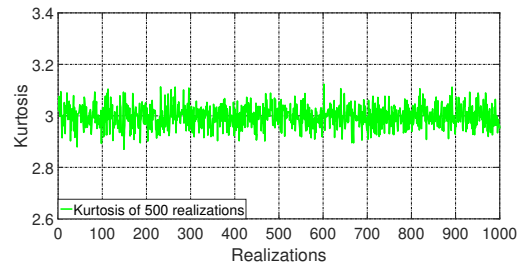
(a) Mean ( $R_{sc} = 100\Omega$ )



(b) Variance ( $R_{sc} = 100\Omega$ )



(c) Skewness ( $R_{sc} = 100\Omega$ )



(d) Kurtosis ( $R_{sc} = 100\Omega$ )

Figure 11: First four statistical moments of the estimated  $I_{sc}$  with  $100\Omega$ 's SC resistance

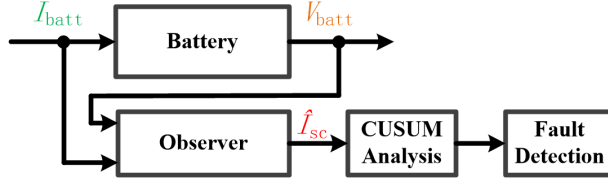


Figure 12: Flowchart of battery SC detection.

where,  $\mu_f$  and  $\mu_h$  are the mean values of  $\hat{I}_{sc}$  in healthy and faulty cases respectively.  $\sigma_h$  is the standard deviation value of  $\hat{I}_{sc}$  in the healthy condition. According to the previous simulation studies,  $\mu_f$  and  $\mu_h$  are selected as 0.03 and 0 respectively.  $\sigma_h^2 = 0.006$ .

Furthermore, the CUSUM decision law can be computed as [38]:

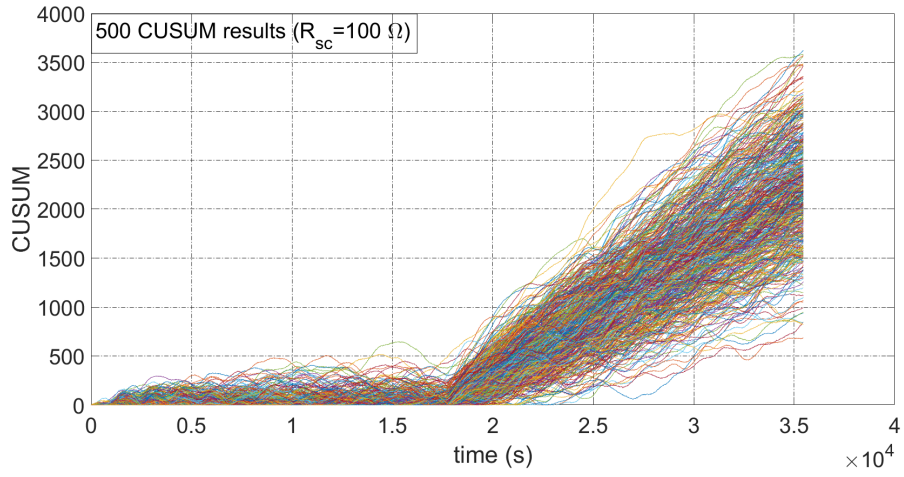
$$D_{S_N} = \left( S_{N_k} - \min_{1 \leq j \leq k} (S_{N_j}) \right) \quad (15)$$

Hence, fault detection method based on the flowchart in Fig. 12 is executed 500 times in healthy condition and 500 times for  $R_{sc} = 100\Omega, 75\Omega, 50\Omega, 25\Omega$  respectively. As it can be seen from Fig. 13, the combination of fault estimator and CUSUM analysis is effective to carry out the incipient SC detection.

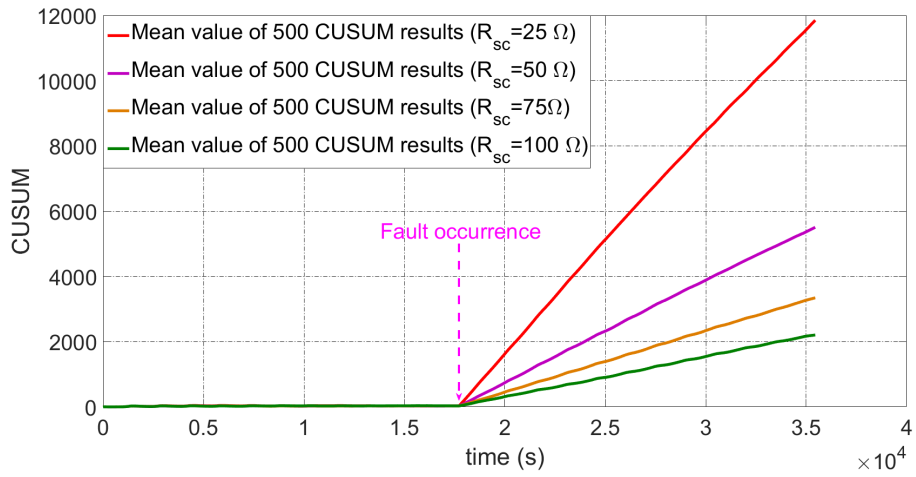
## 5.2. Threshold setting

### 5.2.1. Threshold 1

The first method for setting detection threshold  $T_h$  is to select  $T_h = 0.99 D_{S_N max}$ , where  $D_{S_N max}$  is the maximum value of  $D_{S_N}$  in the healthy case. If CUSUM decision value is higher than  $T_h$ , a SC fault is detected [39]. Hence, according to the 500 simulation results,  $T_h = 640.4445$ .



(a) CUSUM detection results under  $R_{sc} = 100 \Omega$



(b) CUSUM detection results under different SC conditions.

Figure 13: CUSUM detection results

### 5.2.2. Threshold 2

Furthermore, to take advantage of the optimality of CUSUM algorithm, probability density function (PDF) of the mean  $\hat{I}_{sc}$  with and without  $100\Omega$ 's resistance is shown in Fig. 14. Besides, Kolmogorov-Smirnov test is processed to assess the PDF of  $\hat{I}_{sc}$  is Gaussian. Hence, the CUSUM can be the applied optimally [37].

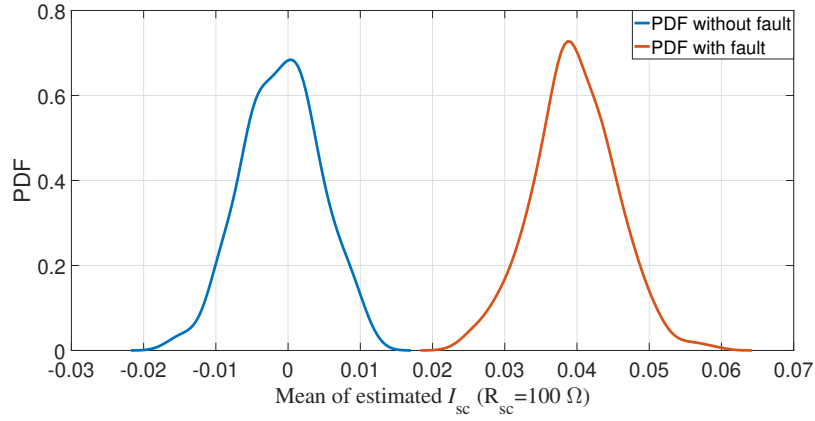


Figure 14: PDF of mean value of estimated  $I_{sc}$  ( $R_{sc} = 100\Omega$ )

Therefore, detection threshold  $T_h$  can be set based on the empirical equation  $T_h = \mu_{cusum} + 3\sigma_{cusum}$  [40]. In our case,  $\mu_{cusum}$  is the mean value of the 500's CUSUM decision mean value,  $\sigma_{cusum}$  is the standard deviation of the 500's CUSUM decision mean value. Therefore,  $T_h = 55.2014$  in this case.

### 5.3. Robustness of fault detection

Robustness of fault detection for  $R_{sc} = 100\Omega$  under different disturbance conditions is evaluated probabilistically with:

- The probability of detection (PD), which represents the ability to correctly detect fault occurrence [39].
- The probability of false alarm (PFA), which measures the probability of considering a healthy situation as a fault [39].

Finally, receiver operating characteristics (ROC) curve can be plotted based on PD and PFA. It is used to demonstrate fault detection method performance under different disturbance conditions. The variance of the disturbance term  $d$  is changed in order to simulate the different disturbance conditions. As shown in Fig. 15, for the different levels of nuisances, CUSUM can detect incipient SC occurrence with a  $PD > 0.9$ .

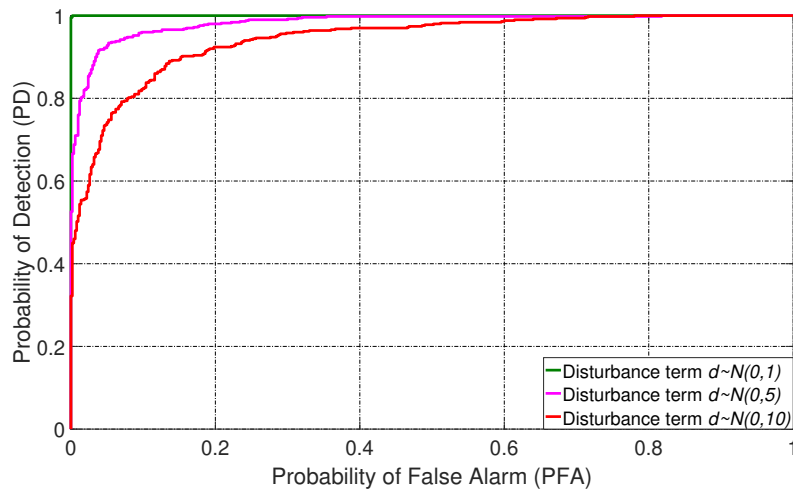


Figure 15: Performance of CUSUM under different disturbance conditions ( $R_{sc} = 100\Omega$ )

## 6. Conclusion

In this paper, battery SC fault detection is treated from the perspective of fault estimation based on an extended equivalent circuit model (ECM) to

take into account the short-circuit (internal or external). Because the battery OCV-SOC curve is non linear, we have first proposed a systematic approach to design the self-regulating mechanism to cope with this non linearity thanks to TS fuzzy system modelling and optimized Gaussian membership functions in different SOC ranges where the OCV-SOC is linear. This approach has two main advantages. Firstly, the model is much simpler compared to classical one that uses a small discretization step. Secondly, the model is more robust because it does not require strong approximation on the linearity of OCV-SOC curve. Thanks to this model, the fault estimator is based on several linear observers combined through a TS fuzzification process. The proposed estimator can provide a reliable and accurate estimation of the battery state of charge even after SC fault occurrence. The mean value of the absolute estimation error for 100  $\Omega$  SC's current is equal to 8.66%. The estimated SC current has been treated as a time-series signal to extract fault feature. We have applied CUSUM analysis on the estimated fault signal to improve fault detection when nuisance level increases. The proposed battery incipient SC detection method is flexible (the model can be adapted to different battery technologies), interoperable (it can be easily combined with thermal and aging models) and is based only on common available measurements (battery current and voltage). The obtained results are very promising with a probability of detection higher than 0.9 for all the cases.

In future work, experimental validation should be conducted to verify simulation results. And battery fault detection information should be included in the energy management strategy.

## References

- [1] T. Bank, S. Klamor, D. U. Sauer, Lithium-ion cell requirements in a real-world 48 v system and implications for an extensive aging analysis, *Journal of Energy Storage* 30 (2020) 101465.
- [2] M. Yue, S. Jemei, R. Gouriveau, N. Zerhouni, Review on health-conscious energy management strategies for fuel cell hybrid electric vehicles: Degradation models and strategies, *International Journal of Hydrogen Energy* 44 (2019) 6844 – 6861.
- [3] J. Meng, M. Boukhnifer, D. Diallo, On-line model-based short circuit diagnosis of lithium-ion batteries for electric vehicle application, in: *IECON 2019-45th Annual Conference of the IEEE Industrial Electronics Society*, volume 1, IEEE, 2019, pp. 6022–6027.
- [4] X. Feng, Y. Pan, X. He, L. Wang, M. Ouyang, Detecting the internal short circuit in large-format lithium-ion battery using model-based fault-diagnosis algorithm, *Journal of Energy Storage* 18 (2018) 26–39.
- [5] P. Shen, M. Ouyang, L. Lu, J. Li, X. Feng, The co-estimation of state of charge, state of health, and state of function for lithium-ion batteries in electric vehicles, *IEEE Transactions on vehicular technology* 67 (2017) 92–103.
- [6] M. Yue, S. Jemei, N. Zerhouni, Health-conscious energy management for fuel cell hybrid electric vehicles based on prognostics-enabled decision-making, *IEEE Transactions on Vehicular Technology* 68 (2019) 11483–11491.

- [7] J. Meng, M. Boukhnifer, D. Diallo, T. Wang, A new cascaded framework for lithium-ion battery state and parameter estimation, *Applied Sciences* 10 (2020) 1009.
- [8] Y. Zhang, R. Xiong, H. He, X. Qu, M. Pecht, Aging characteristics-based health diagnosis and remaining useful life prognostics for lithium-ion batteries, *ETransportation* 1 (2019) 100004.
- [9] C. Yang, X. Wang, Q. Fang, H. Dai, Y. Cao, X. Wei, An online soc and capacity estimation method for aged lithium-ion battery pack considering cell inconsistency, *Journal of Energy Storage* 29 (2020) 101250.
- [10] T. R. Tanim, E. J. Dufek, L. K. Walker, C. D. Ho, C. E. Hendricks, J. P. Christophersen, Advanced diagnostics to evaluate heterogeneity in lithium-ion battery modules, *eTransportation* 3 (2020) 100045.
- [11] M. Ouyang, M. Zhang, X. Feng, L. Lu, J. Li, X. He, Y. Zheng, Internal short circuit detection for battery pack using equivalent parameter and consistency method, *Journal of Power Sources* 294 (2015) 272–283.
- [12] X. Kong, Y. Zheng, M. Ouyang, L. Lu, J. Li, Z. Zhang, Fault diagnosis and quantitative analysis of micro-short circuits for lithium-ion batteries in battery packs, *Journal of Power Sources* 395 (2018) 358–368.
- [13] A. Sidhu, A. Izadian, S. Anwar, Adaptive nonlinear model-based fault diagnosis of li-ion batteries, *IEEE Transactions on Industrial Electronics* 62 (2014) 1002–1011.
- [14] X. Feng, M. Ouyang, X. Liu, L. Lu, Y. Xia, X. He, Thermal runaway

- mechanism of lithium ion battery for electric vehicles: A review, *Energy Storage Materials* 10 (2018) 246–267.
- [15] X. Feng, C. Weng, M. Ouyang, J. Sun, Online internal short circuit detection for a large format lithium ion battery, *Applied Energy* 161 (2016) 168–180.
- [16] S. Dey, Z. A. Biron, S. Tatipamula, N. Das, S. Mohon, B. Ayalew, P. Pisu, Model-based real-time thermal fault diagnosis of lithium-ion batteries, *Control Engineering Practice* 56 (2016) 37–48.
- [17] X. Kong, G. L. Plett, M. S. Trimboli, Z. Zhang, D. Qiao, T. Zhao, Y. Zheng, Pseudo-two-dimensional model and impedance diagnosis of micro internal short circuit in lithium-ion cells, *Journal of Energy Storage* 27 (2020) 101085.
- [18] R. Xiong, R. Yang, Z. Chen, W. Shen, F. Sun, Online fault diagnosis of external short circuit for lithium-ion battery pack, *IEEE Transactions on Industrial Electronics* 67 (2019) 1081–1091.
- [19] Z. Chen, R. Xiong, J. Tian, X. Shang, J. Lu, Model-based fault diagnosis approach on external short circuit of lithium-ion battery used in electric vehicles, *Applied energy* 184 (2016) 365–374.
- [20] T. Reichl, P. Hrzina, Capacity detection of internal short circuit, *Journal of Energy Storage* 15 (2018) 345–349.
- [21] W. Gao, Y. Zheng, M. Ouyang, J. Li, X. Lai, X. Hu, Micro-short-circuit diagnosis for series-connected lithium-ion battery packs using

- mean-difference model, *IEEE Transactions on Industrial Electronics* 66 (2018) 2132–2142.
- [22] S. M. M. Alavi, S. Fekriasl, S. N. Niyakan, M. Saif, Fault detection and isolation in batteries power electronics and chargers, *Journal of Energy Storage* 25 (2019) 100807.
- [23] R. Xiong, X. Gong, C. C. Mi, F. Sun, A robust state-of-charge estimator for multiple types of lithium-ion batteries using adaptive extended kalman filter, *Journal of Power Sources* 243 (2013) 805–816.
- [24] Z. Chen, Y. Fu, C. C. Mi, State of charge estimation of lithium-ion batteries in electric drive vehicles using extended kalman filtering, *IEEE Transactions on Vehicular Technology* 62 (2012) 1020–1030.
- [25] W. Waag, C. Fleischer, D. U. Sauer, Critical review of the methods for monitoring of lithium-ion batteries in electric and hybrid vehicles, *Journal of Power Sources* 258 (2014) 321–339.
- [26] Z. Zhang, X. Kong, Y. Zheng, L. Zhou, X. Lai, Real-time diagnosis of micro-short circuit for li-ion batteries utilizing low-pass filters, *Energy* 166 (2019) 1013–1024.
- [27] S. Zhao, S. R. Duncan, D. A. Howey, Observability analysis and state estimation of lithium-ion batteries in the presence of sensor biases, *IEEE Transactions on Control Systems Technology* 25 (2016) 326–333.
- [28] J. Meng, M. Boukhniifer, D. Diallo, Comparative study of lithium-ion battery open-circuit-voltage online estimation methods, *IET Electrical Systems in Transportation* 12 (2020) 162–169.

- [29] H. Rahimi-Eichi, F. Baronti, M.-Y. Chow, Online adaptive parameter identification and state-of-charge coestimation for lithium-polymer battery cells, *IEEE Transactions on Industrial Electronics* 61 (2013) 2053–2061.
- [30] B. Xia, Z. Zhang, Z. Lao, W. Wang, W. Sun, Y. Lai, M. Wang, Strong tracking of a h-infinity filter in lithium-ion battery state of charge estimation, *Energies* 11 (2018) 1481.
- [31] K. Zhang, B. Jiang, V. Cocquempot, Fuzzy unknown input observer-based robust fault estimation design for discrete-time fuzzy systems, *Signal Processing* 128 (2016) 40–47.
- [32] K. Zhang, B. Jiang, V. Cocquempot, H. Zhang, A framework of robust fault estimation observer design for continuous-time/discrete-time systems, *Optimal control applications and methods* 34 (2013) 442–457.
- [33] B. Shafai, M. Saif, Proportional-integral observer in robust control, fault detection, and decentralized control of dynamic systems, in: *Control and Systems Engineering*, Springer, 2015, pp. 13–43.
- [34] G. Du, W. Cao, S. Hu, Z. Lin, T. Yuan, Design and assessment of an electric vehicle powertrain model based on real-world driving and charging cycles, *IEEE Transactions on Vehicular Technology* 68 (2019) 1178–1187.
- [35] Y.-H. Chiang, W.-Y. Sean, J.-C. Ke, Online estimation of internal resistance and open-circuit voltage of lithium-ion batteries in electric vehicles, *Journal of Power Sources* 196 (2011) 3921–3932.

- [36] C. Depature, S. Jemei, L. Boulon, A. Bouscayrol, N. Marx, S. Morando, A. Castaings, Ieee vts motor vehicles challenge 2017-energy management of a fuel cell/battery vehicle, in: 2016 IEEE Vehicle Power and Propulsion Conference (VPPC), IEEE, 2016, pp. 1–6.
- [37] M. Basseville, I. V. Nikiforov, et al., Detection of abrupt changes: theory and application, volume 104, prentice Hall Englewood Cliffs, 1993.
- [38] C. Delpha, D. Diallo, H. Al Samrout, N. Moubayed, Multiple incipient fault diagnosis in three-phase electrical systems using multivariate statistical signal processing, Engineering Applications of Artificial Intelligence 73 (2018) 68–79.
- [39] M. Baghli, C. Delpha, D. Diallo, A. Hallouche, D. Mba, T. Wang, Three-level npc inverter incipient fault detection and classification using output current statistical analysis, Energies 12 (2019) 1372.
- [40] A. Youssef, C. Delpha, D. Diallo, An optimal fault detection threshold for early detection using kullback–leibler divergence for unknown distribution data, Signal Processing 120 (2016) 266–279.